CHAPTER

Spintronics 11

CHAPTER OUTLINE

11.1 INTRODUCTION

As we noted in Chapter 10 on electronics, charges are manipulated by electric fields, but spins are generally ignored. Magnetic recording and other techniques use the spin only through the magnetization of a ferromagnet. When giant magnetoresistance (GMR) of the magnetic multilayers was discovered in 1988, an efficient control of the electrons was achieved through the orientation of their magnetization by acting on their spin. The application of the GMR to the read heads of the hard discs contributed significantly to the quick rise in the density of stored information. This led to the extension of hard disc technology and consumer electronics.

A large number of phenomena related to the control and manipulation of spin currents were developed through a new area of physics/materials science called spintronics. The rapidly growing area of research in spintronics includes such phenomena as spin transfer, molecular spintronics, spintronics with semiconductors, and single-electron spintronics.

Physics of Condensed Matter. DOI: 10.1016/B978-0-12-384954-0.00011-6

11.2 MAGNETORESISTANCE

In Chapter 3, we discussed the Hall effect by considering a conductor in the shape of a rod that has a rectangular cross-section, which is placed under a magnetic field **B** in the z direction. There is a longitudinal electric field E_x. The electric and magnetic fields are so adjusted that the current cannot flow out of the rod in the y direction $(j_y = 0)$. The charges pile up on the surface of the sample, thereby setting up an electric field E_y. This field, which nullifies the Lorentz force (Eq. 3.90), is known as the Hall field. The Hall coefficient R_H, which defines the size of the carrier, is defined as $R_H = E_y/Bj_x$. The component of the resistivity tensor ρ, ρ_{yx}, is the Hall resistance defined as $\rho_{yx} = E_y/j_x$, whereas the diagonal component ρ_{xx} is the magnetoresistance, defined as

$$\rho_{xx} = \frac{E_x}{j_x}, \tag{11.1}$$

and the magnetoresistance ratio is defined as

$$\frac{\Delta\rho}{\rho_0} = \frac{\rho - \rho_0}{\rho_0}, \tag{11.2}$$

where ρ and ρ_0 are the resistivities (along a given direction) in the presence and absence of a magnetic field, respectively. The dependence of the electrical resistance of the material on an applied magnetic field, usually perpendicular to the direction of the current, represents this effect.

11.3 GIANT MAGNETORESISTANCE

11.3.1 Metallic Multilayers

A typical multilayer unit is shown in Figure 11.1. In a magnetic multilayer system, one of the metals (A) is magnetic, whereas the other (B) is nonmagnetic, which is referred to as the spacer layer. When the thickness of the spacer layer is varied, there are oscillations in the magnetic coupling between the magnetic layers. The thickness of these thin films can vary from a few tenths of a nanometer to tens of nanometers. The magnetization directions of the ferromagnetic layers are coupled to each other through an exchange interaction. The sign of this coupling oscillates as the thickness of the spacer layer is varied. The best multilayer samples have around 30 periods of oscillations.

Some metallic multilayers exhibit drastic changes in magnetoresistance and, hence, the name giant magnetoresistance (GMR). The drastic change of magnetoresistance in metallic multilayers has resulted in a new definition of the magnetoresistance ratio, MR, as

$$MR = \frac{R_{AP} - R_P}{R_P} \times 100, \tag{11.3}$$

where R_P and R_{Ap} are the resistances of the parallel and antiparallel magnetic configurations, respectively.

In the mid-1980s, it became possible to develop molecular-beam epitaxy (MBE) and other techniques to fabricate multilayers composed of very thin individual layers. The explanation of the

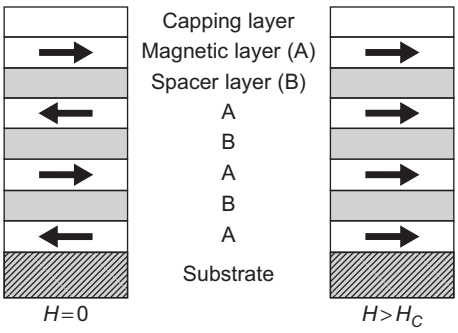

FIGURE 11.1

A multilayer structure and the changes in magnetization directions with an applied magnetic field **H**. The parallel magnetizations lead to a large magnetoresistance compared to that of an antiparallel structure.

Reproduced from Fernando[6] with the permission of Elsevier.

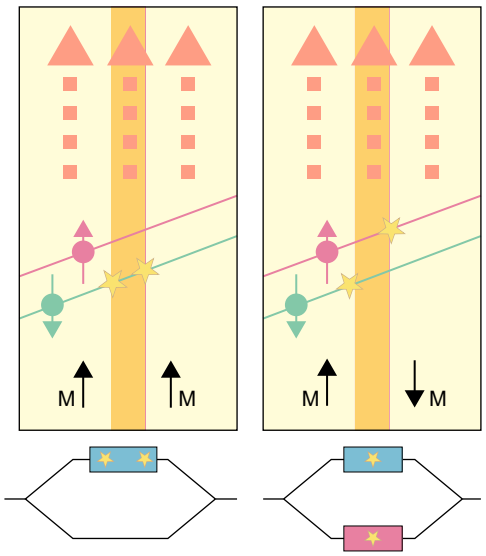

FIGURE 11.2

Spin-dependent electron scattering and redistribution of scattering events upon anti-alignment of magnetization.

Reproduced from Grunberg[11] with the permission of the American Physical Society.

GMR effect includes spin-dependent electron scattering and redistribution of scattering events due to anti-alignment of magnetizations. This scenario is shown in Figure 11.2.

The microscopic explanation for the GMR effect is that the scattering rates of the electrons depends on the orientation (parallel or antiparallel) of the electron spins with respect to the local magnetizations. Figure 11.2 shows two structures, one with parallel and the other with antiparallel alignment with the magnetization. The electrons with spin parallel to the local magnetization in their random walk are not scattered in the ideal situation. In Figure 11.2, only one passage from the left to the right is shown as a sample of the electron motion. A short circuit is caused by the electrons that are not scattered. However, when the electron with spin-up enters the layer where the magnetization has been turned around, its spin is opposite to the local magnetization. The bottom diagram in Figure 11.2 shows the increase in resistivity due to the removal of the short circuit. In practice, although both types of electrons are scattered, the resistivity due to the antiparallel magnetization is more than that due to parallel magnetization.

In Figure 11.3, the arrows represent the majority spin direction in the magnetic layers. In the ferromagnetic (F) configuration, the spin+ $(s_z = 1/2)$ electrons are weakly scattered everywhere, which gives a short circuit effect and hence a small resistivity. In the antiferromagnetic (AF) configuration, each spin direction is scattered at every second magnetic layer, and the resistivity is higher because there is no short circuit effect.

The short circuit effect for the ferromagnetic (F) configuration is visually explained in Figure 11.4. In the parallel (P) configuration, majority electrons in the (+) channel $(s_z = 1/2)$ experience little or

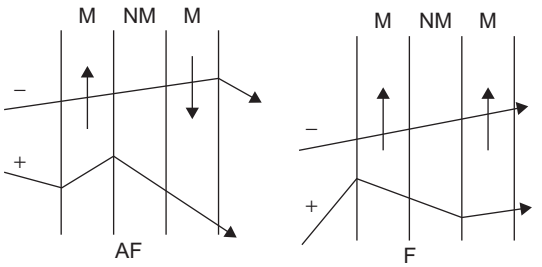

FIGURE 11.3

Schematic picture of the electron trajectories. The electron trajectories between two scatterings are represented by straight lines and the scatterings by abrupt change in direction. The + and – are for electron spins $s_z = 1/2$ and $s_z = -1/2$, respectively.

Reproduced from Fert et al.[10] with the permission of Elsevier.

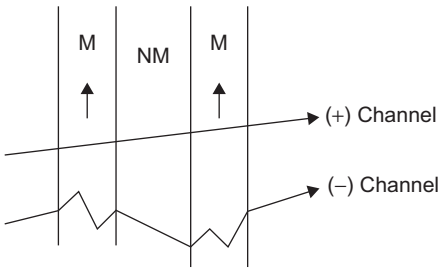

FIGURE 11.4

Schematic diagram of the short circuit effect.

Reproduced from Fernando[6] with the permission of Elsevier.

no resistance, and hence, a short circuit effect occurs. In the antiparallel (AP) configuration (not shown), electrons in the (+) and (–) ($s_z = -1/2$) channels will experience a significant resistance when going through the slab with opposite magnetization with no short circuit effects.

11.4 MOTT'S THEORY OF SPIN-DEPENDENT SCATTERING OF ELECTRONS

A simple model of a scattering of electrons, which was given by Mott[15] will be presented here. It was modified later by more complex models. We consider a ferromagnetic *d*-band metal with a magnetization $M(T)$ at temperature T. The schematic density of states representing *s*-, *p*-, and *d*-bands of a transition metal is shown in Figure 11.5.

If M_0 is the saturation magnetization at $T=0$, and $\beta = M(T)/M_0$, a fraction $(1-\beta)/2$ of the unoccupied *d* states will have their spins parallel to M, and a fraction $(1+\beta)/2$ will have their spins antiparallel. If we define $\rho_1(E)$ and $\rho_2(E)$ as the respective density of states, then they will have a parabolic form,

$$\rho_1(E) = a\sqrt{(E_1 - E)} \tag{11.4}$$

and

$$\rho_2(E) = a\sqrt{(E_2 - E)}, \tag{11.5}$$

where E_1 and E_2 are the highest energies the two spins can have. However, above the Curie temperature, where the system becomes paramagnetic

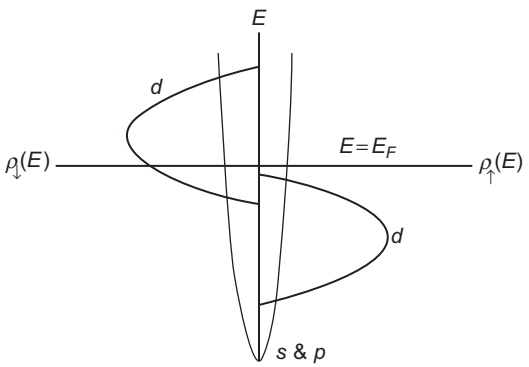

FIGURE 11.5

Density of states plotted against E for *s*, *p*, and *d* states of a transition metal.

and the number of parallel spins equals the number of antiparallel spins, $E_1 = E_2 = E_0$. It can be shown that the corresponding relaxation times are related to the density of states as

$$\frac{1}{\tau_1} \propto \rho_1(E) + \delta \tag{11.6}$$

and

$$\frac{1}{\tau_2} \propto \rho_2(E) + \delta, \tag{11.7}$$

where δ is a contribution from spin-independent scattering. From Eqs. (11.4) through (11.7), it can be shown that (Problem 11.1)

$$\frac{1}{\tau_1} = A(T/M_I\theta^2)\left[\frac{\sqrt{(E_1 - E)}}{\sqrt{(E_0 - \zeta_0)}} + \alpha\right] \tag{11.8}$$

and

$$\frac{1}{\tau_2} = A(T/M_I\theta^2)\left[\frac{\sqrt{(E_2 - E)}}{\sqrt{(E_0 - \zeta_0)}} + \alpha\right], \tag{11.9}$$

where $\alpha \approx 1/4$, θ is the Debye temperature, and A is a constant. If ζ_0 represents the energy at $T = 0$ and $\beta = 0$, and ζ_0' represents the energy at the highest occupied state (Fermi energy) at $T = 0$ when the states are split, because the density of states is proportional to $n_0^{1/3}$, we can write (Problem 11.2)

$$\sqrt{\frac{E_1 - \zeta_0'}{E_0 - \zeta_0}} = (1 - \beta)^{1/3} \tag{11.10}$$

and

$$\sqrt{\frac{E_2 - \zeta_0'}{E_0 - \zeta_0}} = (1 + \beta)^{1/3}. \tag{11.11}$$

One can write the expression for conductivity by using a Drude-type formula, but including the energy dependence of the relaxation time,

$$\sigma = -Ne^2/m \int \frac{(\tau_1 + \tau_2)}{2} \frac{\partial f}{\partial E} dE. \tag{11.12}$$

The resistivity $\rho(\beta, T) = 1/\sigma$ is obtained by approximating the partial derivative of the integrand in Eq. (11.12) to be nonzero only when $E = \zeta_0'$. We obtain, after some algebra (Problem 11.3),

$$\rho(\beta, T) = A(T/m\theta^2)\left[\frac{1}{(1 - \beta)^{1/3} + \alpha} + \frac{1}{(1 + \beta)^{1/3} + \alpha}\right]^{-1}. \tag{11.13}$$

Because $\alpha \simeq 0.25$, the ratio of the resistances between the saturated magnetization case ($\beta = 1$) and the paramagnetic case ($\beta = 0$) is given by

$$\frac{\rho(\beta = 1, T)}{\rho(\beta = 0, T)} \simeq 0.34. \tag{11.14}$$

If we define the resistances for up and down channels as $R^{\uparrow}$ and $R^{\downarrow}$, then the resistances R_P and R_{AP} for the parallel and antiparallel alignments of spins relative to a given magnetic layer are given by

$$R_P = (1/R^{\uparrow} + 1/R^{\downarrow})^{-1} \tag{11.15}$$

and

$$R_{AP} = (R^{\uparrow} + R^{\downarrow})/4, \tag{11.16}$$

when the mean path of the electrons is much higher than the repeat length of the multilayer. From Eqs. (11.3), (11.15), and (11.16), we obtain

$$\mathrm{MR} = \frac{(1-\eta)^2}{4\eta} \times 100\%, \tag{11.17}$$

where

$$\eta = \frac{R_{\downarrow}}{R_{\uparrow}}. \tag{11.18}$$

Because η is a positive parameter, it follows from Eq. (11.17) that $R_{AP} > R_P$. This is a very simplified explanation of the higher resistance encountered in the antiparallel case.

When an applied field changes an alignment from antiferromagnetic (AF) to ferromagnetic (F) alignment, the difference in resistivity is the largest. The AF alignment is usually provided by interlayer exchange or by coercivities of successive magnetic layers, by pinning the magnetization using an antiferromagnetic material in direct contact, known as exchange biasing. If GMR is obtained by exchange biasing, it is called a spin-valve system.

The first discovery of GMR was done by Baibich et al.[1] on Fe/Cr magnetic multilayers, in which it is possible to switch the relative orientation in adjacent magnetic layers from antiparallel to parallel by applying a magnetic field. The resistivity is strongly enhanced in the antiparallel magnetic configuration of two adjacent layers A and B because the electrons in each channel are slowed down at every second magnetic layer. There is no such enhancement in layers A and B in the parallel magnetic configuration because the electrons can go easily through all the magnetic layers, and the short circuit through this channel leads to a small resistance. This opens up the possibility of switching between high and low resistivity states by changing the relative orientation of the magnetizations of A and B layers from parallel to antiparallel. Similar GMR effects were discovered by Binash et al.[2] in Fe/Cr/Fe trilayers. These effects are shown later in Figure 11.9. Camley and Barnas[3] presented a theoretical description of the GMR effects in Fe/Cr/Fe trilayers by calculating the resistivity using Boltzmann transport equations, with spin-dependent scattering at the interface.

11.5 CAMLEY–BARNAS MODEL

The Camley–Barnas model[3] includes the idea that there is an antiferromagnetic coupling between Fe films due to the intervening Cr films. At the zero field, the resulting magnetic moments of neighboring Fe films are antiparallel to each other. However, in a strong external magnetic field, all the magnetic moments of the Fe films can be forced to lie in the same direction. Earlier experimental results suggested that the resistance is the largest when the magnetic moments in neighboring Fe films are antiparallel and smallest when they are parallel. Further, multilayer structures with thin Fe films have a much larger magnetoresistance than a single sandwich structure of Fe/Cr/Fe. In addition, the magnetoresistance is increased by a factor of 2 or 3 when the temperature is changed from room temperature to that of liquid He. Camley and Barnas interpreted these results to conclude that a spin-dependent scattering is responsible for the observed effects and the relative lengths of the mean-free path are more important than the thickness of the various films.

To develop a theory for the multilayer, Camley and Barnas first considered a single sandwich structure of Fe/Cr/Fe, as shown in Figure 11.6, and computed the conductivity by using the Boltzmann equation.

In Figure 11.6, the dashed line in the center of the Cr films is the position at which the change in axis of quantization for the electron spin is calculated. In each region, the Boltzmann equation reduces to a differential equation that depends on the coordinate z only,

$$\frac{\partial g}{\partial z} + \frac{g}{\tau v_z} = \frac{eE}{mv_z}\frac{\partial f_0}{\partial v_x}, \tag{11.19}$$

where f_0 is the equilibrium distribution function, τ is the relaxation time, E is the external field in the x direction, and g is the correction to the distribution function due to scattering.

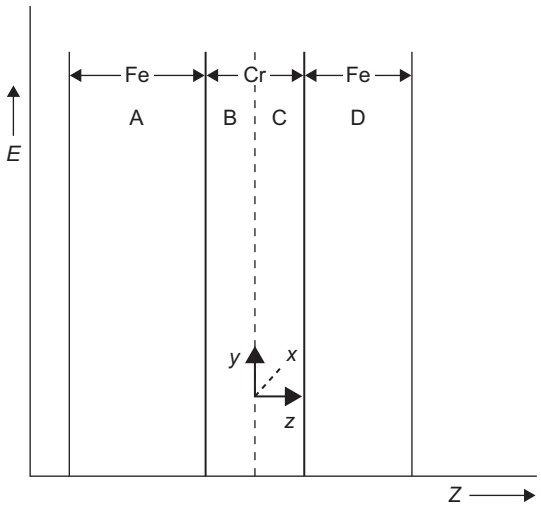

FIGURE 11.6

The geometry of the Fe/Cr/Fe sandwich structure.

In the region A, the contributions to g for regions for spin-up or spin-down electrons moving to the right (positive v_z) or left (negative v_z) are

$$g = g_{A+\uparrow}(v_z, z) + g_{A+\downarrow}(v_z, z) \tag{11.20}$$

and

$$g = g_{A-\uparrow}(v_z, z) + g_{A-\downarrow}(v_z, z). \tag{11.21}$$

From Eqs. (11.19) through (11.21), it can be easily shown that (Problem 11.4)

$$g_{A\pm\uparrow}(v_z, z) = \frac{eE\tau}{m}\frac{\partial f_0}{\partial v_x}\left[1 + A_{\pm\uparrow}\exp\left(\frac{\mp z}{\tau|v_z|}\right)\right] \tag{11.22}$$

and

$$g_{A\pm\downarrow}(v_z, z) = \frac{eE\tau}{m}\frac{\partial f_0}{\partial v_x}\left[1 + A_{\pm\downarrow}\exp\left(\frac{\mp z}{\tau|v_z|}\right)\right]. \tag{11.23}$$

The coefficients $A_{\pm\uparrow(\downarrow)}$ and similar coefficients for the regions B, C, and D are determined through the boundary conditions. The distribution function g for an electron leaving the surface (at the outer surfaces of the sandwich) is equal to the distribution function g for an electron of the same spin striking the surface multiplied by a specular scattering event R_0. Thus, we obtain

$$g_{A+\uparrow} = R_0 g_{A-1} \text{ at } z = -b \tag{11.24}$$

and

$$g_{D-\uparrow} = R_0 g_{D+\uparrow} \text{ at } z = +b. \tag{11.25}$$

Similar equations are obtained for down-spins.

Camley and Barnas[3] assumed a model system of two equivalent simple metals that have the same Fermi energies, mean-free path values, and so on. They neglected the angular dependence of scattering and assumed that there is only transmission or diffusive scattering at the Fe/Cr interfaces. They further assumed that the scattering at the outer boundaries is purely diffusive (the reflection coefficients are zero). If the transmission coefficients are $T_\uparrow$ for up-spins and $T_\downarrow$ for down-spins, for up-spins at $z = -a$,

$$g_{A-\uparrow(\downarrow)} = T_{\uparrow(\downarrow)} g_{B-\uparrow(\downarrow)} \tag{11.26}$$

and

$$g_{B+\uparrow(\downarrow)} = T_{\uparrow(\downarrow)} g_{A+\uparrow(\downarrow)}. \tag{11.27}$$

A similar set of equations holds for the $z=+a$ interface. Similar boundary conditions are obtained for $g_{B-\uparrow(\downarrow)}$ and $g_{C-\uparrow(\downarrow)}$, except that one has to account for the fact that the magnetic moments in the two films are in different directions by an angle θ, which is the angle between the magnetization vectors in the two Fe films. We define the transmission coefficients,

$$T_{\uparrow\uparrow} = T_{\downarrow\downarrow} = \cos^2(\theta/2) \tag{11.28}$$

and

$$T_{\uparrow\downarrow} = T_{\downarrow\uparrow} = \sin^2(\theta/2), \tag{11.29}$$

where $T_{\uparrow\uparrow}$ is the probability of an electron of spin-up (in layer A, with respect to the magnetization) at $z = -0$ to continue as a spin-up (in layer D, with respect to magnetization) at $z = 0$, and the other symbols are defined similarly. We obtain

$$g_{B-\uparrow(\downarrow)} = g_{C-\uparrow(\downarrow)} \cos^2(\theta/2) + g_{C-\downarrow(\uparrow)} \sin^2(\theta/2) \tag{11.30}$$

and

$$g_{C+\uparrow(\downarrow)} = g_{B+\uparrow(\downarrow)} \cos^2(\theta/2) + g_{B+\downarrow(\uparrow)} \sin^2(\theta/2). \tag{11.31}$$

The current density at different fields are obtained by using the expression

$$J(z) = \int v_x g(v_x, z)\, d^3v. \tag{11.32}$$

The current of the whole structure is obtained by integrating $J(z)$ over the coordinate z.
Camley and Barnas defined the diffusive scattering parameter,

$$D_\uparrow = 1 - T_\uparrow, \tag{11.33}$$

and the asymmetry in up-spin and down-spin scattering,

$$N = D_\uparrow / D_\downarrow. \tag{11.34}$$

Their results are plotted in Figure 11.7.

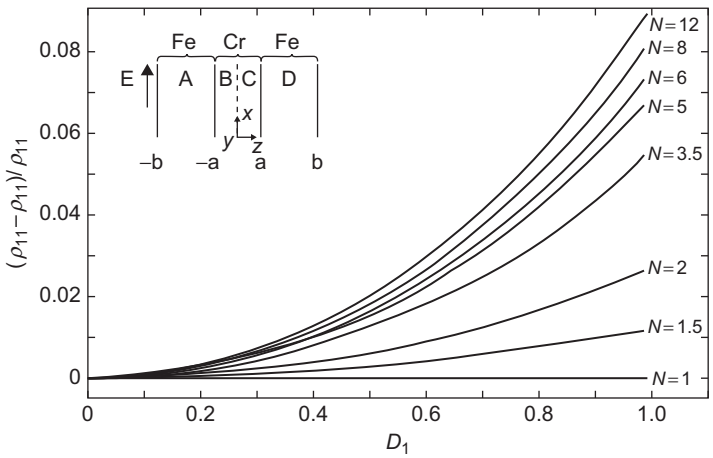

FIGURE 11.7

The maximum normalized change in resistance as a function of D_1 and N. The inset shows the geometry shown in Figure 11.6.

Reproduced from Camley and Barnas[3] with the permission of the American Physical Society.

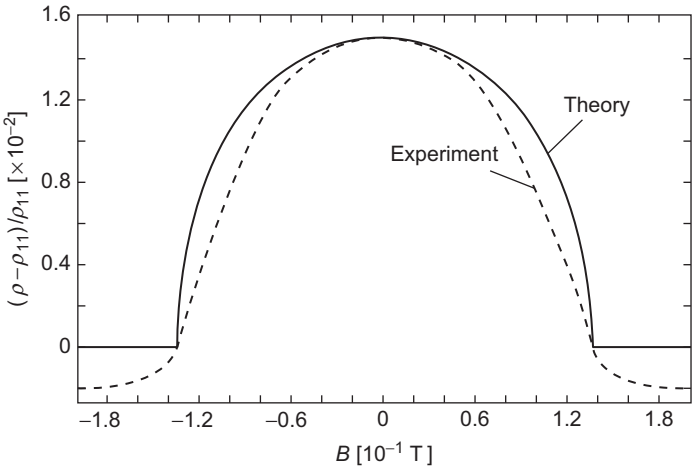

FIGURE 11.8

The percentage change of resistance as a function of an applied field ($N = 6$, $D_1 = 0.48$). The experimental results are from Binash et al.[2] from Figure 11.9b.

Reproduced from Camley and Barnas[3] with the permission of the American Physical Society.

The calculations shown in Figure 11.7 were made to show how the magnetoresistance effect depends on $D_\uparrow$ and N for a (120 Å Fe)/(10 Å Cr)/(120 Å Fe) sandwich structure with a mean-free path of $\lambda = 180$ Å. The theoretical value of the percentage change in resistance as a function of an applied field for a (120 Å Fe)/(10 Å Cr)/(120 Å Fe) sandwich structure is shown in Figure 11.8.

In the preceding calculations, the mean-free path is $\lambda = 180$ Å, and the angle θ between the magnetizations in the two Fe films was calculated by minimizing the sum of the exchange, anisotropy, and Zeeman energies for the Fe/Cr/Fe sandwich.

The first observation of giant magnetoresistance was discovered by Baibich et al.[1] and is shown in Figure 11.9a. It may be noted that if we define $\text{MR} = (R_{AP} - R_P)/R_P \times 100$, MR = 85% for the (Fe 3 nm/Cr 0.9 nm) multilayer. The experimental results of Binash et al.[2] for Fe/Cr/Fe trilayers is shown in Figure 11.9b. A schematic diagram of the electrons in parallel (low resistance) and antiparallel (high resistance) spin configurations is shown in Figure 11.9c.

As we noted earlier, GMR can be obtained in the current in plane (CIP) and current perpendicular to plane (CPP) geometry. At present, the CIP configuration is used for most sensor applications, and in most experiments the current flows in the CIP geometry. However, Pratt et al.[17] showed that for the Ag/Co multilayers, CPP-MR is several times larger than the CIP-GMR. There has been considerable interest in CPP-MR, which is more likely to be used in future sensor applications.

11.6 CPP-GMR

11.6.1 Introduction

The first experiment of CPP-GMR was done by sandwiching a magnetic multilayer between superconducting electrodes. This restricted the use of such multilayers only at very low temperatures. However, Fert and Piraux[9] as well as other groups have fabricated magnetic nanowires by electrodepositing into

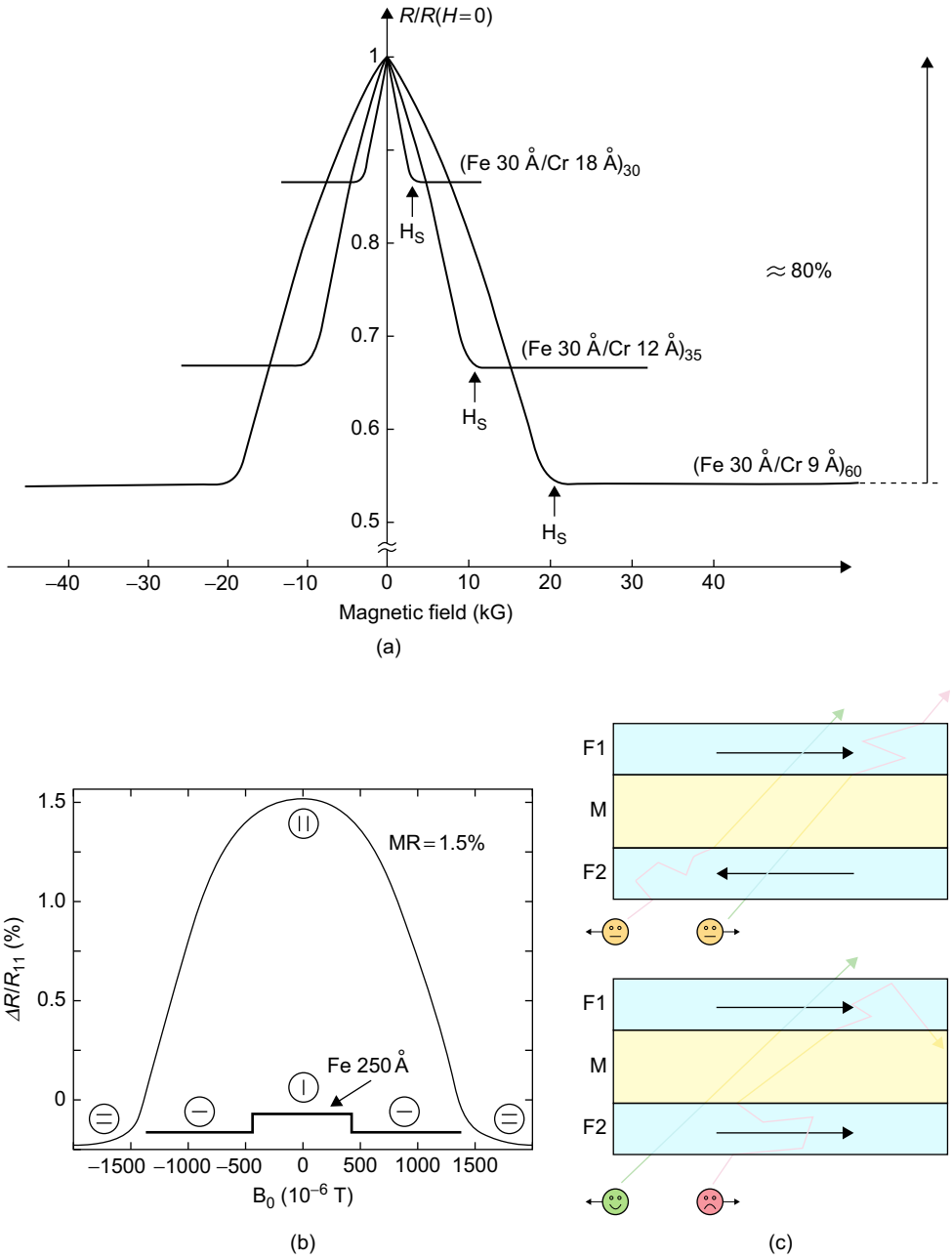

FIGURE 11.9

(a) GMR in Fe/Cr(001) multilayers. MR = 85% for the (Fe 3 nm/Cr 0.9 nm) multilayer. (b) GMR in Fe/Cr/Fe trilayers. (c) Schematic of the mechanism of GMR.

Reproduced from Fert[7] with the permission of American Physical Society.

pores of membranes. These nanowires usually have a diameter in the range 30–500 nm for a length of 10 μm. The multilayered nanowires can be composed of a stack of layers of different metals with thicknesses in the nanometer range.

The general technique for fabrication of magnetic multilayered nanowires in nanoporous polymer membranes (Figure 11.10b) consists of a pulse-plating method in which two metals are deposited from a single solution by switching between the deposition potential of two constituents. These types of multilayers include Co/Cu, NiFe/Cu, Ni/Cu, and Fe/Cu. Other types of multilayered nanowires such as Ni/NiO/Co heterostructures and Co/Pb multilayers have been grown by electrodeposition. We will now summarize the theory of the perpendicular magnetoresistance in magnetic multilayers (CPP-MR) derived by Valet and Fert[22] (the V–F model) and in magnetic nanowires by Fert and Piraux.[9]

11.6.2 Theory of CPP-GMR of Multilayered Nanowires

The V–F theory uses the Boltzmann equation to calculate the transport properties of magnetic multilayers for currents perpendicular to the layer. Their model takes into account both volume and interface scattering and includes a spin-lattice relaxation term τ_{sf}, which describes the relaxation of spin accumulation by spin-flip scattering. The data on the perpendicular magnetoresistance can be used to separate the volume and interface scattering. The notations generally used in the calculation of the magnetoresistance of a multilayer are as follows. The spin ↑ (majority) and spin ↓ (minority) resistivities of the ferromagnetic metal are defined by

$$\rho^F_{\uparrow(\downarrow)} = 2\rho^*_F[1-(+\beta)], \tag{11.35}$$

where β is the bulk-scattering spin asymmetry coefficient. The (equal) spin resistivities of the nonmagnetic metal are defined by

$$\rho^N_{\uparrow(\downarrow)} = 2\rho^*_N, \tag{11.36}$$

and the interface resistances per unit area, $r_\uparrow$ and $r_\downarrow$, are defined by

$$r_{\uparrow(\downarrow)} = 2r^*_b[1-(+)\gamma], \tag{11.37}$$

where γ is the interface asymmetry coefficient, t_N and t_f are defined as the thickness, and l^N_{sf} and l^F_{sf} as the spin diffusion length (SDL) of the nonmagnetic and ferromagnetic layers, respectively. In the long SDL limit, where $t_N \ll l^N_{sf}$ and $t_F \ll l^F_{sf}$, Valet and Fert[22] showed that the resistances R^P (parallel) and R^{AP} (antiparallel) of a unit area of the multilayer (which is also valid for nanowires for a true antiparallel configuration and for a state with zero net magnetization in a volume of the cube of the SDL) are

$$R^{AP} = N(\rho^*_F t_F + \rho^*_N t_N + 2r^*_b) \tag{11.38}$$

and

$$R^P = R^{AP} - \frac{\{\beta\rho^*_F t_F + 2\gamma r^*_b\}^2 N2}{R^{AP}}, \tag{11.39}$$

where N is the number of periods.

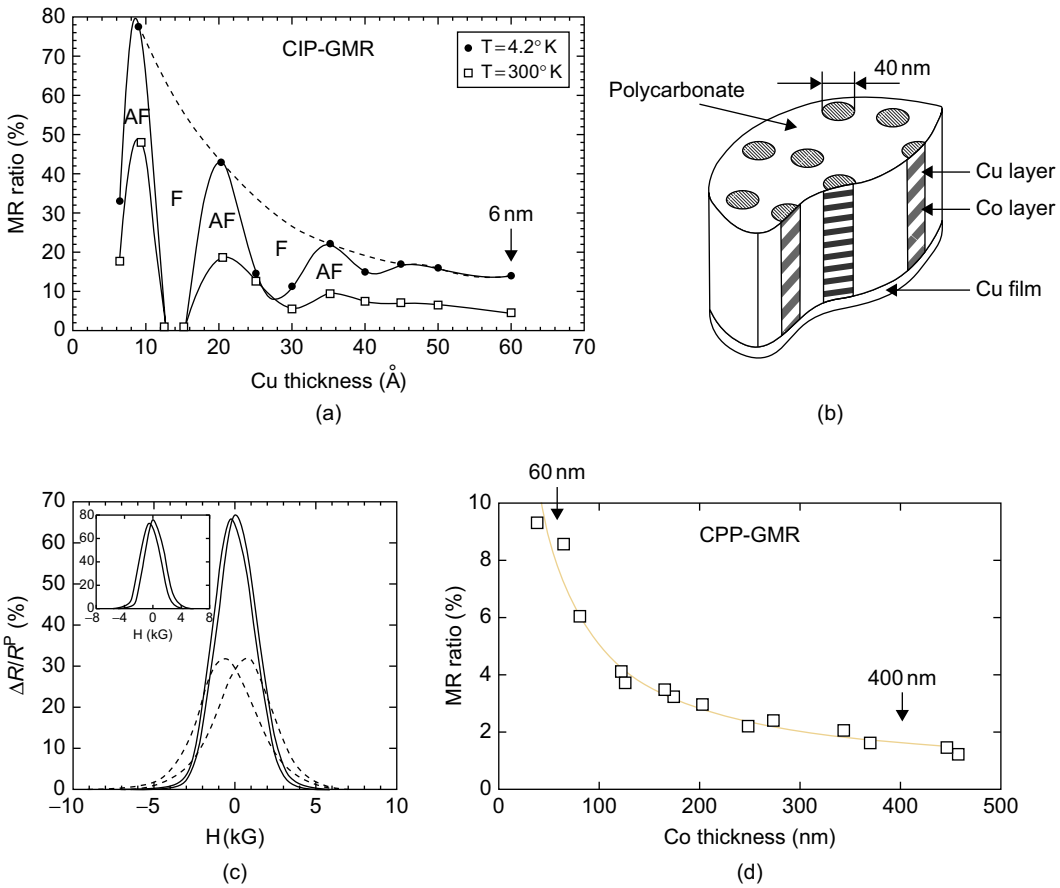

FIGURE 11.10

(a) Variation of the GMR ratio of Co/Cu multilayers as a thickness of Cu in the CIP geometry. (b) Schematic of an array of multilayered nanowires in nanoporous track-etched polymer membranes. (c) The variation of the CPP-GMR ($\Delta R/R^P$) at 77° K for $Ni_{80}Fe_{20}$(12 nm)/Cu(4 nm) (solid lines) and Co(10 nm)/Cu(5 nm) (dotted lines) multilayered nanowires as a function of H. The inset shows the same plot at 4.2° K for the $Ni_{80}Fe_{20}$/Cu sample. (d) Variation of the CPP-GMR ratio of Co/Cu multilayered nanowires as a thickness of the Co layers.

Reproduced from Fert[7] with the permission of the American Physical Society.

From Eqs. (11.38) and (11.39), it can be shown that (Problem 11.5)

$$\left(\frac{R^{AP}-R^{P}}{R^{AP}}\right)^{-1/2}=\frac{\rho_F^* t_F+2r_b^*}{\beta\rho_F^* t_F+2\gamma r_b^*}+\frac{\rho_N^* t_N}{\beta\rho_F^* t_F+2\gamma r_b^*}. \tag{11.40}$$

The magnetoresistance properties of multilayered nanowires helps considerably in the understanding of the CPP-GMR and the determination of the spin diffusion length. In addition, in current-induced

switching (or reversal) of magnetization, nanowires can be used. They are ideal for high-injection density currents in order to probe the change in spin configuration of multilayers.

In Figure 11.10a, the large and oscillatory GMR effects in Co/Cu, which were discovered simultaneously by Mosca et al.[13] and Parkin et al.[16], are shown. In fact, these effects became the archetypical GMR system. In 1991, Dieny et al.[5] observed the GMR in spin valves, i.e., trilayered structures in which the magnetization of one magnetic layer is pinned by coupling with the antiferromagnetic layer while the magnetization by the second layer is free. A small magnetic field can reverse the magnetization of the free layer; this concept is now used in most applications in spin valves.

Figure 11.10b shows a schematic picture of an array of multilayered nanowires in nanoporous track-etched polymer membranes and the technique of fabrication, the theory of which was described earlier. Due to the spin accumulation effects that occur in the CPP geometry, the length scale of the spin transport becomes the long spin diffusion length. In fact, the CPP-GMR has demonstrated the spin accumulation effects that determine the propagation of a spin-polarized current through magnetic and nonmagnetic materials. The CPP-GMR plays an important role in all recent developments of spintronics.

As one can see in Figures 11.10c and d, in the CPP, the GMR is not only higher than in CIP, but also subsists in multilayers with relatively thick layers, up to the micron range. The CPP-GMR has demonstrated the spin accumulation effects that govern the propagation of a spin-polarized current through a series of magnetic and nonmagnetic materials. Thus, it plays an important role in the development and future use of spintronics. The key mechanism driving a spin-polarized current at a large distance from the interface is the diffusion current induced by the accumulation of spins at the magnetic–nonmagnetic interface. For example, spin-polarized currents can be transported in long carbon nanotubes because the SDL is quite large beyond the micron range.

When an electron flux crosses the interface between a ferromagnetic and a nonmagnetic material, far from the magnetic side, the current is large in one of the spin channels. However, when the flux is far from the interface on the other side, the current is equally distributed in both channels. This scenario is shown in Figure 11.11.

Figure 11.11a shows the spin-up and spin-down currents far from an interface between ferromagnetic and nonmagnetic conductors outside the spin accumulation zone. Figure 11.11b shows the splitting of the chemical potentials $E_{F\uparrow}$ and $E_{F\downarrow}$ at the interface. When the current travels through the spin-accumulation zone, it is polarized due to the inversion of the spin accumulation and opposite spin flips. The spin flips control the gradual depolarization of the current due to the left and the right. Figure 11.11c shows the variation of the current spin polarization on both sides of metal/metal, where there is a balance between the spin flips on both sides, and the metal/nonmagnetic semiconductor (without spin-dependent interface resistance), where the spin flips dominate in the left side. Thus, the current is nearly depolarized when it enters the semiconductor. One can introduce a tunnel junction, which results in a discontinuity of the spin accumulation at the interface, thereby increasing the depolarization from the metallic to the semiconductor side. However, due to the large tunnel resistances, it is difficult to efficiently transform the spin information into an electrical signal.

11.7 MTJ, TMR, AND MRAM

There have been significant advances in the research on the tunneling magnetoresistance (TMR) of magnetic tunnel junctions (MTJ). The MTJs are tunnel junctions with ferromagnetic electrodes of which the resistances are different for parallel and antiparallel configurations. In addition, the two

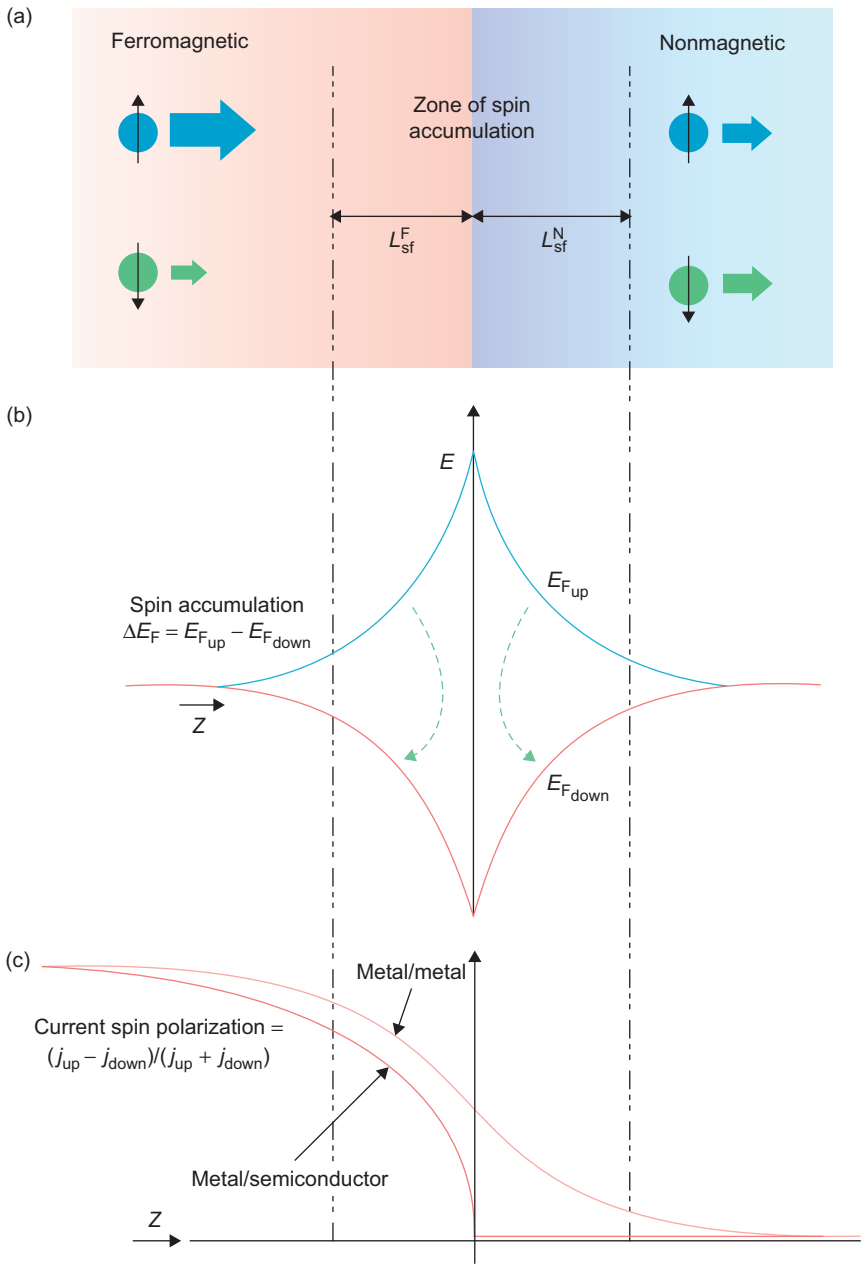

FIGURE 11.11

Schematic representation of the spin accumulation at an interface between a ferromagnetic and a nonmagnetic layer.

Reproduced from Fert[7] with the permission of the American Physical Society.

metallic layers that are called electrodes are separated by an insulating layer thin enough to allow some tunneling current. Julliere[13] did one of the early experiments on MTJ by using the Fe-Ge-Co system. The conductance G(V) measurements, made for Fe and Co when the average magnetizations were parallel and antiparallel, showed a difference related to the spin polarizations of the tunneling conduction electrons. Julliere used a simple (stochastic) model for tunneling electrons and denoted the fractions of electrons, of which the magnetic moments are parallel to the magnetizations in Fe and Co, as a and a'. The conductance of the Fe-Ge-Co junction when the magnetizations in Fe and Co are parallel (G_p) and antiparallel (G_{AP}) can be expressed as[21]

$$G_p \propto [aa' + (1-a)(1-a')] \tag{11.41}$$

and

$$G_{ap} \propto [a(1-a') + a'(1-a)]. \tag{11.42}$$

Assuming that the spin is conserved,

$$\text{TMR} = \frac{G_P - G_{ap}}{G_{ap}} = \frac{2PP'}{(1-PP')}, \tag{11.43}$$

where the conduction electron spin polarization of the two ferromagnetic metals are[13]

$$P = 2a - 1 \quad \text{and} \quad P' = 2a' - 1\,. \tag{11.44}$$

The original value measured by Julliere was 14%, mainly due to interface roughness. Recent experiments indicate that in MTJs consisting of ferromagnetic amorphous CoFeB and MgO, the TMR can be as large as 500%. In fact, it appears that MgO is crucial for achieving large TMR values.

The polarization of tunneling electrons depends on the barrier height of the insulator in addition to the polarization of the ferromagnets. Slonczewski[19] made the simple assumption that the ferromagnets had parabolic but spin-split bands that are separated by an insulating barrier. The schematic picture is shown in Figure 11.12. A schematic picture of the one- and two-band parabolic models is shown in Figure 11.13.

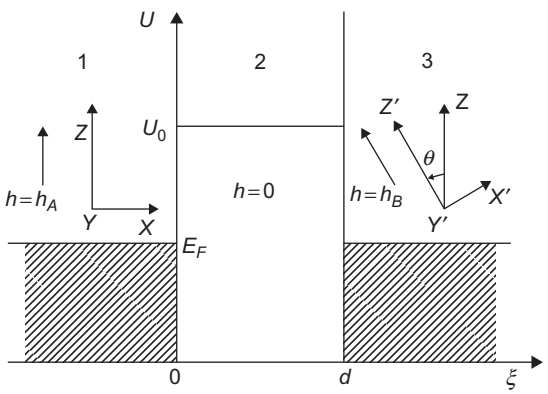

FIGURE 11.12

Schematic picture of an insulator between two different types of ferromagnets.

Reproduced from Slonczewski[19] with the permission of the American Physical Society.

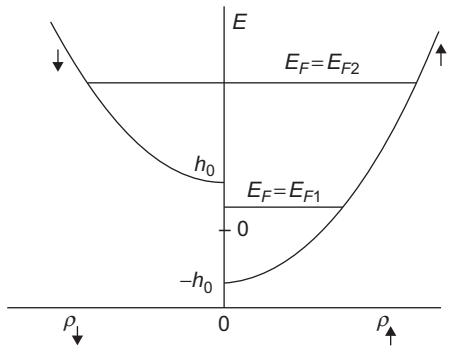

FIGURE 11.13

Density of spin-up ($\rho_\uparrow$) and spin-down ($\rho_\downarrow$) electrons. The positions of the Fermi energy for one-band (E_{F1}) and two-band (E_{F2}) models of a ferromagnet are shown schematically.

Reproduced from Slonczewski[19] with the permission of the American Physical Society.

When the barrier has low energy and thin size, the wave function of the two ferromagnets has to be matched at the interfaces. Slonczewski[19] showed that P', the polarization of the tunneling electrons, depends on the polarization of the ferromagnets as well as on the barrier height,

$$P' = \left[\frac{k^\uparrow - k^\downarrow}{k^\uparrow + k^\downarrow}\right]\left[\frac{\kappa^2 - k^\uparrow k^\downarrow}{\kappa^2 + k^\uparrow k^\downarrow}\right], \tag{11.45}$$

where $k^\uparrow$ and $k^\downarrow$ are the Fermi wave vectors for the up- and down-spin bands, and

$$\hbar\kappa = \sqrt{[2m(V_b - E_F]}, \tag{11.46}$$

where V_b is the barrier height, and E_F is the Fermi level of the ferromagnet. This barrier-dependent factor can vary from -1 to 1. It may be noted that for parabolic, free electron bands, the polarization associated with the ferromagnets is

$$P = \left[\frac{k^\uparrow - k^\downarrow}{k^\uparrow + k^\downarrow}\right]\left[\frac{\rho^\uparrow - \rho^\downarrow}{\rho^\uparrow + \rho^\downarrow}\right]. \tag{11.47}$$

Thus, Eqs. (11.46) and (11.47) change Julliere's result obtained in Eq. (11.44), especially when the tunnel barrier is high. The signs of the polarization can even change in certain cases.

The magnetic random access memory (MRAM) is built from the concept of MTJs, as shown in Figure 11.14.

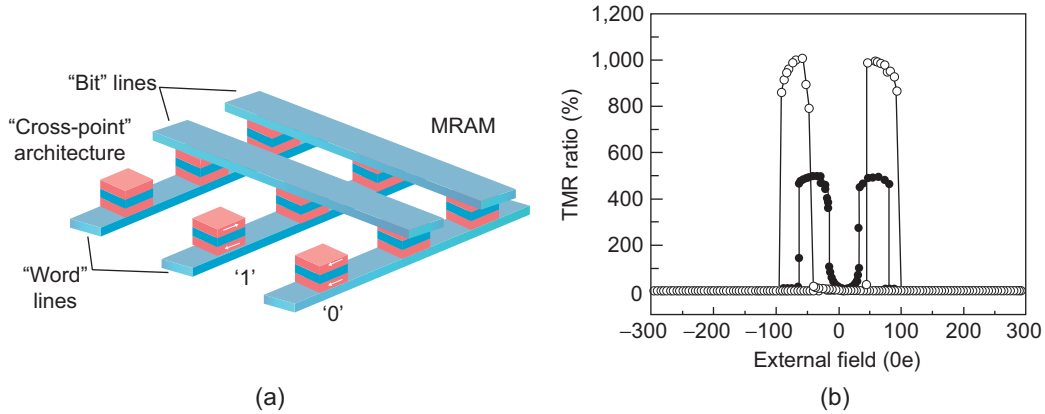

FIGURE 11.14

Principles of the magnetic random access memory (MRAM) in the basic "cross-point" structure.

Reproduced from Fert[7] with the permission of the American Physical Society.

In Figure 11.14a, the binary information "0" and "1" is recorded on the two opposite orientations of the magnetization of the MTJs, which are connected to two crossing points of two perpendicular arrays of parallel conducting lines. The current pulses are sent through one line of each array for "writing," and only at the crossing point, the resulting magnetic field is high enough to orient the magnetization of the free layer. The resistance between the two lines between the addressed cell is measured for "reading." Figure 11.14b shows the TMR $= (R_{\max} - R_{\min})/R_{\min}$ for the stack $(Co_{25}Fe_{75})_{80}B_{20}(4\text{ nm})/MgO(2.1\text{ nm})/(Co_{25}Fe_{75})_{80}B_{20}(4.3\text{ nm})$ annealed at 475°C after growth. The measurements were done at room temperature (closed circles) and low temperatures (open circles). In the first MRAMs, the memory cells are MTJs with an alumina barrier. The "word" and "bit" lines generate magnetic fields that switch the magnetic configuration. The future of the technology of computers is based on the ST-RAM, which is based on MgO tunnel junctions and switching by spin transfer.

11.8 SPIN TRANSFER TORQUES AND MAGNETIC SWITCHING

A spin current, $\overleftrightarrow{\mathbf{Q}}$, which consists of moving spins, can be written as

$$\overleftrightarrow{\mathbf{Q}} = (\hbar/2)P\hat{\mathbf{s}} \otimes \mathbf{j}, \tag{11.48}$$

where P is the polarization (scalar). The spin and current densities can be written as

$$\overrightarrow{\mathbf{s}}(\mathbf{r}) = \sum_{i\sigma\sigma'} \psi^*_{i\sigma}(\mathbf{r})\hat{\mathbf{S}}_{\sigma,\sigma'}\psi^*_{i\sigma'}(\mathbf{r}) \tag{11.49}$$

and

$$\overleftrightarrow{\mathbf{Q}}(\mathbf{r}) = \sum_{i\sigma\sigma'} \mathrm{Re}(\psi^*_{i\sigma}(\mathbf{r})\hat{\mathbf{S}}_{\sigma,\sigma'} \otimes \hat{\mathbf{v}}\psi^*_{i\sigma}(\mathbf{r})), \tag{11.50}$$

where $\hat{\mathbf{S}}_{\sigma,\sigma'}$ and $\hat{\mathbf{v}}$ are spin and velocity operators. The continuity equation, which expresses the conservation of number of electrons, is given by

$$\frac{\partial n}{\partial t} = -\nabla \cdot \mathbf{j}, \tag{11.51}$$

where n is the number density, and $\mathbf{j}$ is the current density. It can be shown that there is a similar equation for the spin density, $\mathbf{s}$, which consists of an extra term arising due to the noncommutivity of spin density with magnetocrystalline anisotropy,

$$\frac{\partial \mathbf{s}}{\partial t} = -\nabla \cdot \overleftrightarrow{\mathbf{Q}} + \mathbf{n}_{ext}, \tag{11.52}$$

where $\nabla \cdot \overleftrightarrow{\mathbf{Q}} = \partial_k Q_{ik}$. Here, $\mathbf{n}_{ext}$ is the external torque density that rotates the spins. Eq. (11.52) is equivalent to the continuity equation stated in Eq. (11.51) with additional terms $\mathbf{n}_{ext}$. In general, there are two contributions to the spin current. If the direction of magnetization is nonuniform in a ferromagnet, the left and right spin currents do not cancel, and the gradient of this current gives rise to a spin torque $\mathbf{n}_{ex} = -\nabla \cdot \overleftrightarrow{\mathbf{Q}}_{ex}$. There is also a second contribution to the spin current at the interfaces due to the imbalance in the population of the spin states at or near the Fermi energy. It can be

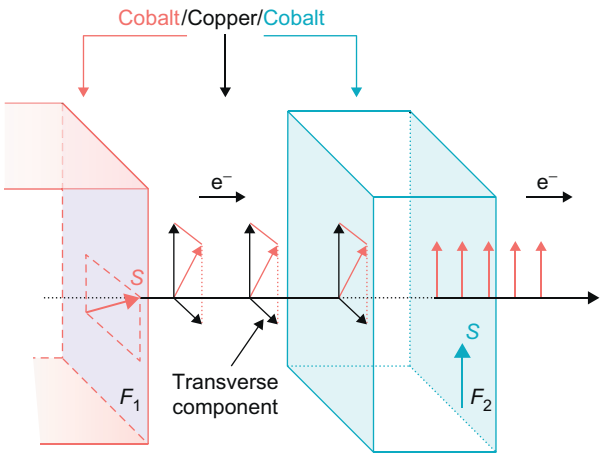

FIGURE 11.15

Illustration of the spin-transfer concept. The spin-transfer torque described previously acts on F_2.

Reproduced from Fert[7] with the permission of the American Physical Society.

shown that the spin current along the direction of the magnetization is conserved. Further, the reflected and transmitted components do not (generally) have any transverse components. Therefore, the main mechanism for transfer of angular momentum is the exchange interaction experienced by the electrons in the ferromagnet, which exerts a torque on the spin current. The scattering of spin at a ferromagnetic interface is a growing area of research, and we have considered only an elementary discussion of this topic.

To summarize, in spin-transfer phenomena, the magnetic moments of a ferromagnet are manipulated by the transfer of spin-angular momentum from a spin-polarized current without the application of a magnetic field. The transfer of a transverse spin current to a "free" magnetic layer F_2 is due to the torque acting on the magnetic moment, as briefly described previously. The spin torque can induce irreversible switching of the magnetic moment or can generate precession of the moment in the microwave frequency range in the presence of a magnetic field in a second regime.

This scenario is schematically shown in Figure 11.15. The first magnetic layer, F, prepares a spin-polarized current with an obliquely oriented spin polarization with respect to the magnetization axis of a second layer, F_2. When this current goes through F_2, the exchange interaction aligns its spin polarization along the magnetization axis. Because the exchange interaction is spin conserving, the transverse spin polarization lost by the current is transferred to the total spin of F_2. This can lead to a magnetic switching of the F_2 layer or to magnetic oscillations in the microwave frequency range.

11.9 SPINTRONICS WITH SEMICONDUCTORS

11.9.1 Introduction

Spintronics with semiconductors has the tremendous advantage of combining the potential of the magnetic materials such as the control of current by spin manipulation, nonvolatility, etc., with the potential of the semiconductors (control of current by gate, coupling with optics, etc.). Datta and Das[4]

proposed the concept of a spin-effect transistor (spin FETs) based on spin transport in semiconductor lateral channels between spin-polarized sources and drains with control of the spin transmission by a field-effective gate. The spin precession can be controlled by spin-orbit coupling. The three ingredients for a spin transistor are (1) long relaxation time of a semiconductor, (2) gate voltage control of the spin-orbit coupling, and (3) high spin injection coefficients. Optical experiments have established that electron spins of semiconductors have long relaxation time. Modulation of the spin-orbit splitting at the Fermi level by gate voltage has been reported for both electrons and holes for a variety of semiconductors. However, the spin injection from a ferromagnetic (FM) source into a semiconductor is a very difficult task and yields a maximum of 1% spin polarization.

The conductivity mismatch between an FM metal emitter and a semiconductor is the primary reason for the difficulty in spin injection. It has been shown that if we define the spin injection coefficient in a diffusive regime, γ, as

$$\gamma \propto \sigma_N/\sigma_F, \tag{11.53}$$

where σ_N and σ_F are the conductivities of a normal (N) and FM contacts, then

$$\sigma_N/\sigma_F \gg 1 \tag{11.54}$$

if N is a paramagnetic metal, and

$$\sigma_N/\sigma_F \ll 1 \tag{11.55}$$

if N is a semiconductor. This explains why the spin injection from an FM source into a paramagnetic metal is very efficient, whereas the same from an FM source to a semiconductor is practically impossible. Rashba[18] showed that tunnel contacts (T) can significantly increase spin injection and solve the problem of the mismatch between the conductivities of a ferromagnetic metal (FM) and a semiconductor (N) microstructure. The tunnel resistance, r_c, should be larger than the competing "effective resistances" making the total contact resistance,

$$r_c \geq L_F/\sigma_F, \quad \min\{L_N, w\}/\sigma_N, \tag{11.56}$$

where L_F and L_N are spin diffusion lengths in the FM and N conductors and w is the width of the N conductor.

11.9.2 Theory of an FM-T-N Junction

Rashba considered a semi-infinite FM $(x < 0)$ and N$(x > 0)$ and assumed that the T contact, at $x = 0$, has different spin conductivities, $\Sigma_\uparrow$ and $\Sigma_\downarrow$, for up- and down-spins, and there is no spin relaxation in it. The currents $j_{\uparrow,\downarrow}(x)$ carried by up- and down-spins can be written as

$$j_{\uparrow,\downarrow}(x) = \sigma_{\uparrow,\downarrow}\, \xi'_{\uparrow,\downarrow}(x), \tag{11.57}$$

where $\xi'_{\uparrow,\downarrow}(x)$ is the space derivative of the electrochemical potentials $\xi_{\uparrow,\downarrow}(x)$, which are related to the nonequilibrium parts $n_{\uparrow,\downarrow}(x)$ of the electron concentrations and $\varphi_F(x)$ in the FM region,

$$\xi_{\uparrow,\downarrow}(x) = (eD_{\uparrow,\downarrow}/\sigma_{\uparrow,\downarrow})n_{\uparrow,\downarrow}(x) - \varphi_F(x). \tag{11.58}$$

Here, $D_{\uparrow,\downarrow}$ are diffusion coefficients, and $\sigma_{\uparrow,\downarrow}$ are conductivities of up- and down-spin electrons. To maintain the charge neutrality under the spin injection conditions,

$$n_{\uparrow}(x) + n_{\downarrow}(x) = 0. \tag{11.59}$$

The continuity equation is

$$j'_{\uparrow}(x) = en_{\uparrow}(x)/\tau_s^F, \tag{11.60}$$

where τ_s^F is the spin-relaxation time. Because the charge is conserved,

$$J = j_{\uparrow}(x) + j_{\downarrow}(x) = \text{constant}. \tag{11.61}$$

Introducing the notations

$$\xi_F(x) = \xi_{\uparrow}(x) - \xi_{\downarrow}(x) \tag{11.62}$$

and

$$j_F(x) = j_{\uparrow}(x) - j_{\downarrow}(x), \tag{11.63}$$

one can show (Problem 11.7) that the diffusion equation can be written as

$$D_F\xi''_F(x) = \xi_F(x)/\tau_s^F, \tag{11.64}$$

where

$$D_F = (\sigma_{\downarrow}D_{\uparrow} + \sigma_{\uparrow}D_{\downarrow})/\sigma_F \tag{11.65}$$

and

$$\sigma_F = \sigma_{\uparrow} + \sigma_{\downarrow}. \tag{11.66}$$

From Eqs. (11.57) through (11.66), it can be shown that (Problem 11.8)

$$\varphi'_F(x) = [(D_{\uparrow} - D_{\downarrow})/D_F](\sigma_{\uparrow}\sigma_{\downarrow}/\sigma_F^2)\xi'_F(x) - J/\sigma_F. \tag{11.67}$$

At $T = 0$, the Einstein relations are

$$e^2D_{\uparrow,\downarrow} = \sigma_{\uparrow,\downarrow}/\rho_{\uparrow,\downarrow}, \tag{11.68}$$

where $\rho_{\uparrow,\downarrow}$ are the densities of states at the Fermi level. One can show (Problem 11.9) from Eqs. (11.65) through (11.68) that

$$e^2D_F = (\sigma_{\uparrow}\sigma_{\downarrow}/\sigma_F)(\rho_F/\rho_{\uparrow}\rho_{\downarrow}) \tag{11.69}$$

and

$$(\rho_{\downarrow}\sigma_{\uparrow} - \rho_{\uparrow}\sigma_{\downarrow})/\rho_F\sigma_F = [(\Delta\sigma/\sigma_F) - (\Delta\rho/\rho_F)]/2. \tag{11.70}$$

It can be easily shown (Problem 11.10) from Eqs. (11.67), (11.69), and (11.70) that

$$\varphi'_F(x) = [(\Delta\sigma/\sigma_F) - (\Delta\rho/\rho_F)]\xi'_F(x)/2 - J/\sigma_F. \tag{11.71}$$

From Eqs. (11.57) and (11.71), it is easy to show that

$$j_F(x) = 2(\sigma_\uparrow\sigma_\downarrow/\sigma_F)\xi'_F(x) + (\Delta\sigma/\sigma_F)J. \tag{11.72}$$

Eqs. (11.64), (11.65), (11.71), and (11.72) are a complete system of bulk equations for the F region. One can also show (Problem 11.11) that

$$\xi_\uparrow(x) + \xi_\downarrow(x) = -[2\varphi_F(x) + (\Delta\rho/\rho_F)\xi_F(x)] \tag{11.73}$$

and

$$n_\uparrow(x) = (\rho_\uparrow\rho_\downarrow/\rho_F)\xi_F(x). \tag{11.74}$$

The equations for the N region can be obtained from the equations for the F region by substituting the following in Eqs. (11.64), (11.67), and (11.72):

$$\sigma_\uparrow = \sigma_\downarrow = \sigma_N/2, \tag{11.75}$$

$$\Delta\rho = \Delta\sigma = 0, \tag{11.76}$$

and

$$D_N = D_\uparrow = D_\downarrow. \tag{11.77}$$

We obtain

$$\begin{aligned} D_N\xi_N(x) &= \xi_N(x)/\tau_s^N, \\ \varphi'_N(x) &= -J/\sigma_N, \end{aligned} \tag{11.78}$$

and

$$j_N(x) = \sigma_N\xi'_N(x)/2. \tag{11.79}$$

In Eqs. (11.77) through (11.79), the symbol N in the prefix has been used for the N region, instead of the prefix F, which was used in the F region in the previous equations. Because there is no spin relaxation at the interface $x=0$, the boundary conditions are $j_\uparrow(x)$ is continuous at $x=0$ and hence $j_F(0) = j_N(0)$. Substituting these in Eqs. (11.72) and (11.79), we obtain

$$\sigma_N\xi'_N(0) - 4(\sigma_\uparrow\sigma_\downarrow/\sigma_F)\xi'_F(0) = 2(\Delta\sigma/\sigma_F)J. \tag{11.80}$$

The currents $j_{\uparrow,\downarrow}(0)$ are related to the conductivities of the T contact,

$$j_{\uparrow,\downarrow}(0) = \Sigma_{\uparrow,\downarrow}(\xi^N_{\uparrow,\downarrow} - \xi_{\uparrow,\downarrow}). \tag{11.81}$$

Using Eq. (11.62) and its equivalent for ξ_N, we can rewrite Eq. (11.81) as

$$\xi_N(0) - \xi_F(0) = -2(\Delta\Sigma/\Sigma)r_cJ + 2r_cj(0), \tag{11.82}$$

where

$$\Delta\Sigma = \Sigma_\uparrow - \Sigma_\downarrow,\ \Sigma = \Sigma_\uparrow + \Sigma_\downarrow \text{ and } r_c = \Sigma/4\Sigma_\uparrow\Sigma_\downarrow. \tag{11.83}$$

From Eq. (11.73), its equivalent for φ_N and Eq. (11.83), we obtain

$$(\varphi_F(0) - \varphi_N(0)) + \frac{\Delta\rho}{2\rho_F}\xi_F(0) = r_c J - \frac{\Delta\Sigma}{\Sigma} r_c j(0). \tag{11.84}$$

Eq. (11.84) implies that even when $r_c = 0$, because $\Delta\rho \neq 0$, there is a finite potential drop at the interface, $[\varphi_F(0) - \varphi_N(0)] \propto J$.

11.9.3 Injection Coefficient

The solutions of Eqs. (11.64) and (11.78) are

$$\xi_F(x) = Ae^{-L_F x} \tag{11.85}$$

and

$$\xi_N(x) = Be^{-L_N x}, \tag{11.86}$$

where

$$L_F = (D_F \tau_s^F)^{1/2} \tag{11.87}$$

and

$$L_N = (D_F \tau_s^N)^{1/2}. \tag{11.88}$$

Here, L_F and L_N are known as the diffusion lengths. Thus, we obtain

$$\xi_N'(0) = -\xi_N(0)/L_N = 2\gamma J/\sigma_N \tag{11.89}$$

and

$$\xi_F'(0) = \xi_F(0)/L_F. \tag{11.90}$$

The injection coefficient is defined as

$$\gamma = j(0)/J. \tag{11.91}$$

If we eliminate $\xi_F(0)$ from Eqs. (11.80) and (11.82), we obtain (Problem 11.14)

$$\gamma = [r_F(\Delta\sigma/\sigma_F) + r_c(\Delta\Sigma/\Sigma)]/r_{FN}. \tag{11.92}$$

Here,

$$r_{FN} = r_F + r_N + r_c, \tag{11.93}$$

$$r_F = L_F\sigma_F/4\sigma_\uparrow\sigma_\downarrow, \tag{11.94}$$

and

$$r_N = L_N/\sigma_N. \tag{11.95}$$

Eq. (11.93) shows that r_c, r_F, and r_N are connected in series. We note that if $r_F = r_N$, $\gamma \sim 1$ if and only if $r_c \geq r_N$, a criterion that can be satisfied for narrow tunnel junctions of the atomic scale. If $r_c \gg r_N$, r_F, $r_{FN} \sim r_c$ from Eq. (11.93). Using this approximation, we obtain (from Eq. 11.92) the injection coefficient $\gamma \approx \Delta\Sigma/\Sigma$. The contact completely determines γ in this regime. Thus, the spin injection coefficient is controlled by the element of an FM-T-N junction having the largest effective resistance.

There are alternate possibilities of spintronics with semiconductors based on the use of ferromagnetic semiconductors such as $Ga_{1-x}Mn_xAs$, where $x \ll 1$. There is a good possibility of controlling the ferromagnetic properties with a gate voltage as well as having large TMR effects.

An alternate approach is the spin accumulation effect due to spin-orbit coupling or anomalous scattering mechanisms. When a spin-unpolarized current flows in a metal, the spin-orbit interaction produces asymmetric scattering of the conduction electrons so that spin-up electrons have a larger probability to be scattered to the right compared to spin-down electrons, and spin-down electrons would tend to scatter to the left more than spin-up electrons. This results in a spin current that is generated in a direction transverse to the direction of the flow of current. If a spin-polarized current is present in a semiconductor, a Hall-like effect can be induced by the spin-orbit coupling without an external field. Zhang[23] derived an expression for the spin Hall effect (SHE) using a semiclassical Boltzmann equation and extending it to the case where the spin diffusion effect is finite. He showed that when the

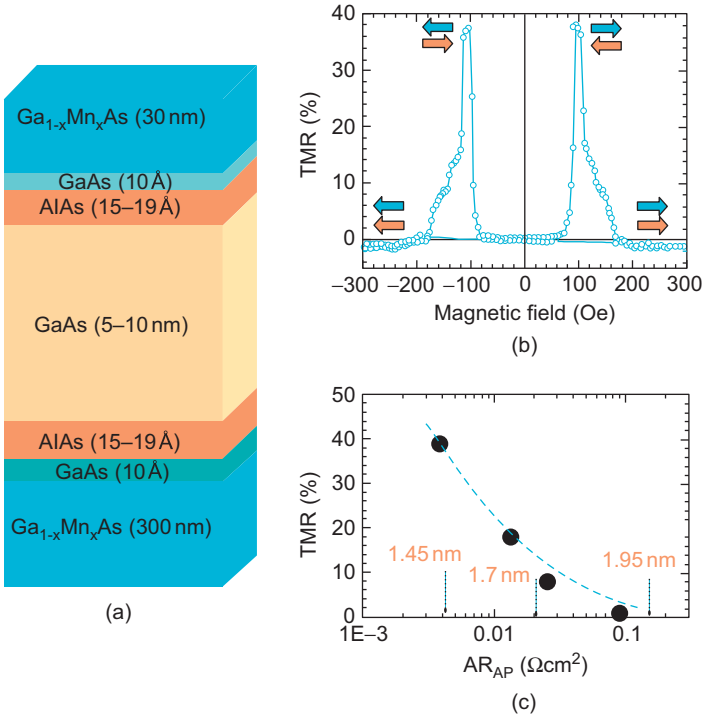

FIGURE 11.16

Spintronics of semiconductors illustrated by experimental results.

Reproduced from Fert[7] with the permission of the American Physical Society.

formulation is applied to certain metals and semiconductors, the magnitude of the spin Hall voltage is much larger than that of magnetic multilayers. Because SHE is also found in nonmagnetic metals, further research in this area is very active.

Spintronics with semiconductors is shown in Figure 11.16. The structure, shown in Figure 11.16a, is composed of a GaAs layer that is separated from the GaMnAs source and drain by tunnel barriers of AlAs. Figure 11.16b shows the MR curve at 4.2° K, which shows a difference in resistance of 40% between the parallel and antiparallel magnetic configuration between the source and the drain. Figure 11.16c shows the MR ratio as a function of the resistance of the tunnel barriers.

It may be noted that spintronics is a very rapidly growing area of research. Recently, large GMR- and TMR-like effects were predicted in carbon-based molecules. In fact, due to small spin-orbit coupling, carbon molecules have a long spin lifetime. Recent experiments on carbon nanotubes between a ferromagnetic source and drain made of the metallic manganite $La_{2/3}Sr_{1/3}MnO_3$ (LSMO) have been encouraging (see Figure 11.17).

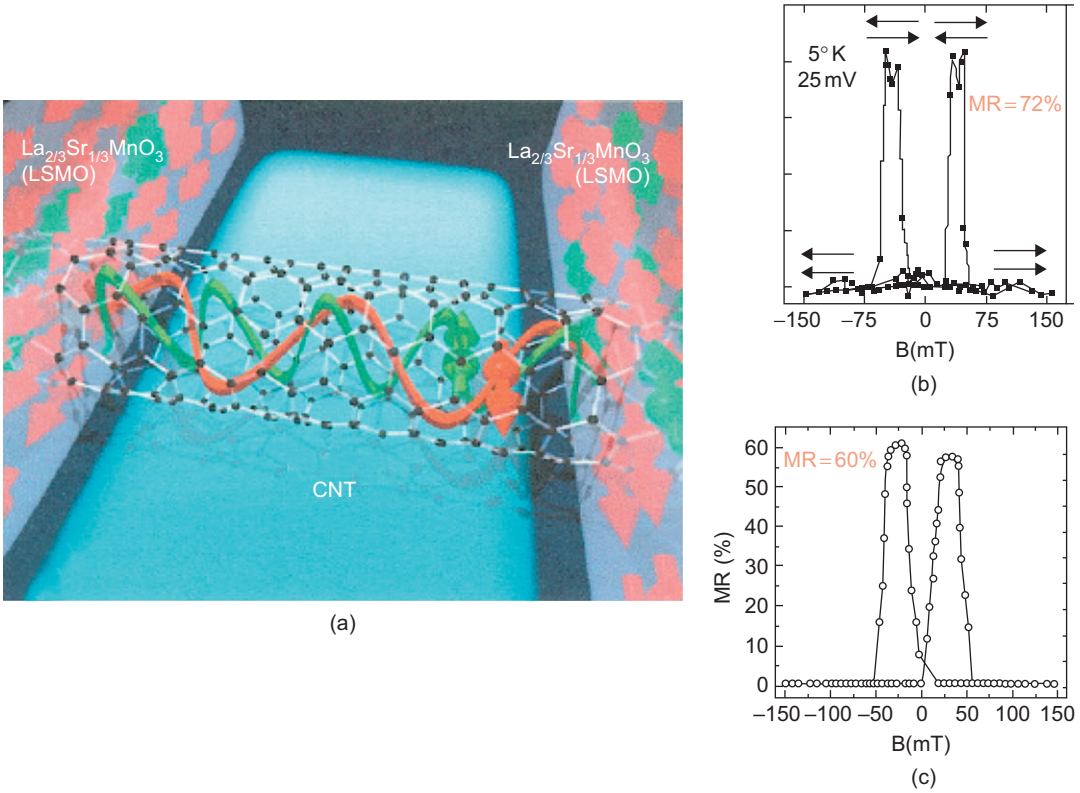

FIGURE 11.17

(a) Sketch of spintronics with LSMO molecules. Magnetoresistance experimental results of Heuso et al.[12] at 4.2°K on carbon nanotubes between electrodes made of LSMO are shown in (b) and (c). A contrast of 72% and 60% is obtained for the parallel (high field) and antiparallel (peaks) magnetic configurations of the source and drain.

Reproduced from Fert[7] with the permission of the American Physical Society.

The results indicate that the resistances of the parallel and antiparallel configurations are between 60% and 70%, which is larger than that obtained for semiconductor channels. In addition, their high Fermi velocity, which is responsible for short dwell time, is an advantage over semiconductors. The research is very active in the general area of spintronics and, in particular, on graphene-based devices.

In view of the above, any review of the general area of spintronics would very quickly become outdated. Therefore, this chapter may be considered as an introduction to the topic.

PROBLEMS

11.1. By using Mott's two-current model, in which the spin transport in a metal is perceived as being due to two independent spin channels, and by using Eqs. (11.4) through (11.7), show that the energy-dependent relaxation times can be expressed as

$$\frac{1}{\tau_1} = A(T/M_I\theta^2)\left[\frac{\sqrt{(E_1 - E)}}{\sqrt{(E_0 - \varsigma_0)}} + \alpha\right] \tag{1}$$

and

$$\frac{1}{\tau_2} = A(T/M_I\theta^2)\left[\frac{\sqrt{(E_2 - E)}}{\sqrt{(E_0 - \varsigma_0)}} + \alpha\right], \tag{2}$$

where $\alpha \approx 1/4$ and θ is the Debye temperature.

11.2. Show that

$$\sqrt{\frac{E_1 - \zeta_0'}{E_0 - \zeta_0}} = (1 - \beta)^{1/3} \tag{1}$$

and

$$\sqrt{\frac{E_2 - \zeta_0'}{E_0 - \zeta_0}} = (1 + \beta)^{1/3}, \tag{2}$$

where ζ_0' represents the energy of the highest occupied state (Fermi energy) at $T = 0$ when the states are split and ζ_0 when $\beta = 0$.

11.3. By using Eqs. (11.8) through (11.12), derive the equation for resistivity (Eq. (11.13),

$$\rho(\beta, T) = A(T/m\theta^2)\left[\frac{1}{(1 - \beta)^{1/3} + \alpha} + \frac{1}{(1 + \beta)^{1/3} + \alpha}\right]^{-1}. \tag{1}$$

11.4. From Eqs. (11.19) through (11.21), show that

$$g_{A\pm\uparrow}(v_z,z)=\frac{eE\tau}{m}\frac{\partial f_0}{\partial v_x}\left[1+A_{\pm\uparrow}\exp\left(\frac{\mp z}{\tau|v_z|}\right)\right] \tag{1}$$

and

$$g_{A\pm\downarrow}(v_z,z)=\frac{eE\tau}{m}\frac{\partial f_0}{\partial v_x}\left[1+A_{\pm\downarrow}\exp\left(\frac{\mp z}{\tau|v_z|}\right)\right]. \tag{2}$$

11.5. We obtained in Eqs. (11.38) and (11.39)

$$R^{AP}=N(\rho_F^*t_F+\rho_N^*t_N+2r_b^*) \tag{1}$$

and

$$R^{P}=R^{AP}-\frac{\{\beta\rho_F^*t_F+2\gamma r_b^*\}^2N^2}{R^{AP}}. \tag{2}$$

Show that

$$\left(\frac{R^{AP}-R^{P}}{R^{AP}}\right)^{-1/2}=\frac{\rho_F^*t_F+2r_b^*}{\beta\rho_F^*t_F+2\gamma r_b^*}+\frac{\rho_N^*t_N}{\beta\rho_F^*t_F+2\gamma r_b^*}. \tag{3}$$

11.6. Using a simple model, we have shown in Eqs. (11.41) and (11.42) that

$$G_p\propto[aa'+(1-a)(1-a')] \tag{1}$$

and

$$G_{ap}\propto[a(1-a')+a'(1-a)]. \tag{2}$$

Assuming that the spin is conserved, show that

$$\text{TMR}=\frac{G_P-G_{ap}}{G_{ap}}=\frac{2PP'}{(1-PP')}, \tag{3}$$

where the conduction electron spin polarization of the two ferromagnetic metals is

$$P=2a-1\quad\text{and}\quad P'=2a'-1\,. \tag{4}$$

11.7. Introducing the notations

$$\xi_F(x)=\xi_\uparrow(x)-\xi_\downarrow(x) \tag{1}$$

and

$$j_F(x)=j_\uparrow(x)-j_\downarrow(x), \tag{2}$$

show that the diffusion equation can be rewritten as

$$D_F \xi''_F(x) = \xi_F(x)/\tau_s^F, \tag{3}$$

where

$$D_F = (\sigma_\downarrow D_\uparrow + \sigma_\uparrow D_\downarrow)/\sigma_F \tag{4}$$

and

$$\sigma_F = \sigma_\uparrow + \sigma_\downarrow. \tag{5}$$

11.8. From Eqs. (11.57) through (11.66), show that

$$\varphi'_F(x) = [(D_\uparrow - D_\downarrow)/D_F](\sigma_\uparrow\sigma_\downarrow/\sigma_F^2)\xi'_F(x) - J/\sigma_F. \tag{1}$$

11.9. By using Eqs. (11.65) through (11.68), show that

$$e^2 D_F = (\sigma_\uparrow\sigma_\downarrow/\sigma_F)(\rho_F/\rho_\uparrow\rho_\downarrow) \tag{1}$$

and

$$(\rho_\downarrow\sigma_\uparrow - \rho_\uparrow\sigma_\downarrow)/\rho_F\sigma_F = [(\Delta\sigma/\sigma_F) - (\Delta\rho/\rho_F)]/2, \tag{2}$$

where

$$\Delta\sigma = \sigma_\uparrow - \sigma_\downarrow, \tag{3}$$

$$\Delta\rho = \rho_\uparrow - \rho_\downarrow, \tag{4}$$

and

$$\rho_F = \rho_\uparrow + \rho_\downarrow. \tag{5}$$

11.10. Show from Eqs. (11.67), (11.69), and (11.70) that

$$\varphi'_F(x) = [(\Delta\sigma/\sigma_F) - (\Delta\rho/\rho_F)]\xi'_F(x)/2 - J/\sigma_F. \tag{1}$$

11.11. From Eqs. (11.64), (11.65), (11.71), and (11.72), show that

$$\xi_\uparrow(x) + \xi_\downarrow(x) = -[2\phi_F(x) + (\Delta\rho/\rho_F)\xi_F(x)] \tag{1}$$

and

$$n_\uparrow(x) = (\rho_\uparrow\rho_\downarrow/\rho_F)\xi_F(x). \tag{2}$$

11.12. Using Eq. (11.62) and its equivalent for ξ_N, show that Eq. (11.81) can be rewritten as

$$\xi_N(0) - \xi_F(0) = -2(\Delta\Sigma/\Sigma)r_c J + 2r_c j(0), \tag{1}$$

where

$$\Delta\Sigma = \Sigma_\uparrow - \Sigma_\downarrow, \Sigma = \Sigma_\uparrow + \Sigma_\downarrow \text{ and } r_c = \Sigma/4\Sigma_\uparrow\Sigma_\downarrow. \quad (2)$$

Here, r_c is the effective contact resistance.

11.13. From Eq. (11.73), its equivalent for φ_N, and Eq. (11.83), show that

$$(\varphi_F(0) - \varphi_N(0)) + \frac{\Delta\rho}{2\rho_F}\xi_F(0) = r_c J - \frac{\Delta\Sigma}{\Sigma} r_c j(0). \quad (1)$$

11.14. The injection coefficient is defined as

$$\gamma = j(0)/J. \quad (1)$$

If one eliminates $\xi_F(0)$ from Eqs. (11.80) and (11.82), show that

$$\gamma = [r_F(\Delta\sigma/\sigma_F) + r_c(\Delta\Sigma/\Sigma)]/r_{FN}. \quad (2)$$

Here,

$$r_{FN} = r_F + r_N + r_c, \quad (3)$$

$$r_F = L_F\sigma_F/4\sigma_\uparrow\sigma_\downarrow, \quad (4)$$

and

$$r_N = L_N/\sigma_N. \quad (5)$$

References

1. Baibich MN, Roole JM, Fert A, Van Dare FN, Petroff F, Etienne P, et al. Giant magnetoresistance of (001)Fe/(001) Cr magnetic superlattices. *Phys Rev Lett* 1988;**61**:2472.
2. Binash G, Grunberg P, Sauerbech F, Zonn W. Enhanced magnetoresistance in layered magnetic structures with antiferromagnetic interlayer exchange. *Phys Rev B* 1989;**39**:4828.
3. Camley RE, Barnas J. Theory of giant magnetoresistance effects in magnetic-layered structures with antiferromagnetic coupling. *Phys Rev Lett* 1989;**63**:662.
4. Datta S, Das B. Electronic analog of the electro-optic modulator. *Appl Phys Lett* 1990;**56**:665.
5. Dieny B, Sperosu VS, Parkin SSP, Gurney BA, Wilhoit DR, Maurri D. Giant magnetoresistance in soft ferromagnetic multilayers. *Phys Rev B* 1991;**43**:1297.
6. Fernando GW. Metallic multilayers and their applications. In: Misra PK, editor. *Handbook of metal physics* (*series*). Amsterdam: Elsevier; 2008.
7. Fert A. Nobel lecture: origin, development, and future of spintronics. *Rev Mod Phys* 2008;**80**:1517.
8. Fert A, Valet T, Barnas J. Perpendicular magnetoresistance in magnetic multilayers. Theoretical model and discussions (invited). *J Appl Phys* 1994;**75**:6693.
9. Fert A, Piraux L. Magnetic nanowires. *J Magn Mag Mater* 1999;**200**:338.

10. Fert A, Gruenberg P, Barthelemey A, Petroff F, Zinn W. Layered magnetic structures: interlayer exchange coupling and giant magnetoresistance. *J Magn Mag Mater* 1995;**140–144**:1.
11. Grunberg PA. Nobel lecture: from spin waves to magnetoresistance and beyond. *Rev Mod Phys* 2008;**80**:1531.
12. Heuso LE, Pruneda JM, Ferrari V, Burnell G, Valdes-Herrere JP, Simmons BD, et al. Transformation of spin information into large electrical signals using carbon nanotubes. *Nature (London)* 2007;**445**:410.
13. Julliere M. Tunneling between ferromagnetic films. *Phys Lett A* 1975;**54**:225.
14. Mosca DH, Petroff F, Fert A, Schroeder PA, Pratt Jr. Jr WP, Laloee T. Oscillatory interlayer coupling and giant magnetoresistance in Co/Cu multilayers. *J Mag Mater* 1991;**94**:L1.
15. Mott N. The resistance and thermoelectric properties of the transition metals. *Proc Roy Soc* 1936;**156**:368.
16. Parkin SSP, Bhadra R, Roche KP. Oscillatory magnetic exchange coupling through thin copper layers. *Phys Rev Lett* 1991;**66**:2152.
17. Pratt Jr. Jr WP, Lee SF, Slaughter JM, Laloee R, Schroeder PA, Bass J. Perpendicular giant magnetoresistance of Ag/Co multilayers. *Phys Rev Lett* 1992;**66**:3060.
18. Rashba EI. Theory of electrical spin injection: tunnel contacts as a solution of the conducting mismatch process. *Phys Rev* 2000;**62**:R 16267.
19. Slonczewski JC. Conductance and exchange coupling of two ferromagnets separated by a tunneling barrier. *Phys Rev B* 1989;**39**:6995.
20. Stiles MD. (a) Exchange coupling in magnetic heterostructures. *Phys Rev B* 1993;**48**:7238; (b) Oscillatory exchange coupling in Fe/Cr multilayers. *Phys Rev B* 1996;**54**:14679.
21. Tedrow PM, Meservy R. Spin-dependent tunneling into ferromagnetic Nickel. *Phys Rev Lett* 1971;**26**:192.
22. Valet T, Fert A. Theory of the perpendicular magnetoresistance in magnetic multilayers. *Phys Rev B* 1993;**48**:7099.
23. Zhang S. Spin hall effect on the presence of spin diffusion. *Phys Rev Lett* 2000;**85**:393.